JOURNAL OF NATURAL PRODUCTS

pubs.acs.org/jnp

Article

Synthesis of [15,15,15-$^2H_3$]-Dihydroartemisinic Acid and Isotope Studies Support a Mixed Mechanism in the Endoperoxide Formation to Artemisinin

Kaitlyn Varela, Hadi D. Arman, and Francis K. Yoshimoto*

Cite This: *J. Nat. Prod.* 2021, 84, 1967−1984

Read Online

ACCESS | Metrics & More | Article Recommendations | Supporting Information

ABSTRACT: Artemisinin is the plant natural product used to treat malaria. The endoperoxide bridge of artemisinin confers its antiparasitic properties. Dihydroartemisinic acid is the biosynthetic precursor of artemisinin that was previously shown to nonenzymatically undergo endoperoxide formation to yield artemisinin. This report discloses the synthesis of [15,15,15-$^2H_3$]-dihydroartemisinic acid and its use to determine the mechanism of endoperoxide formation. Several new observations were made: (i) Ultraviolet-C (UV-C) radiation initially accelerates artemisinin formation and subsequently promotes homolytic cleavage of the O−O bond and rearrangement of artemisinin to a different product, and (ii) dideuterated and trideuterated dihydroartemisinic acid isotopologues at C3 and C15 converted to artemisinin at a slower rate compared to nondeuterated dihydroartemisinic acid, revealing a kinetic isotope effect in the initial ene reaction toward endoperoxide formation ($k_H/k_D \sim 2-3$). (iii) The rate of conversion from dihydroartemisinic acid to artemisinin increased with the amount of dihydroartemisinic acid, suggesting an intermolecular interaction to promote endoperoxide formation, and (iv) $^{18}O_2$-labeling showed incorporation of three and four oxygen atoms from molecular oxygen into the endoperoxide bridge of artemisinin. These results reveal new insights toward understanding the mechanism of endoperoxide formation in artemisinin biosynthesis.

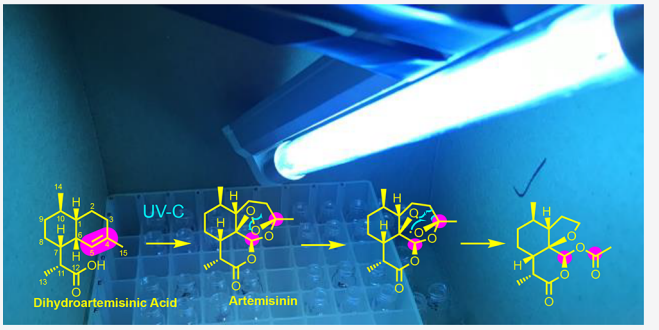

Dihydroartemisinic acid (DHAA)[1] (Figure 1, **1**) is the biosynthetic precursor of artemisinin (**2**), a plant natural product used to treat malaria. The conversion from DHAA to artemisinin is a complex process, which involves: (i) incorporation of an oxygen molecule, (ii) C4−C5 bond cleavage, (iii) incorporation of a second molecule of oxygen, and (iv) polycyclization to form the endoperoxide (Figure 1). The endoperoxide of artemisinin (**2**) is the pharmacophore that triggers the production of reactive oxygen species and leads to the death of the parasite (*Plasmodium falciparum*) that causes malaria.[2,3] Due to its importance in medicine, many research groups have explored the development of new approaches to enable cost-effective methods for artemisinin production.[4−8]

Because the endoperoxide confers the biological activity of artemisinin,[9,10] there is significant interest in determining how the endoperoxide bridge is formed in nature (Figure 1).[11] Although there have been previously reported studies related to exploring the endoperoxide formation in artemisinin biosynthesis through NMR spectroscopy,[12−15] published reports showing the raw data are rare. In particular, Roth and Acton showed oxygen (^{18}O) incorporation into dihydroartemisinic acid hydroperoxide (see Figure 2, nondeuterated version of **4**) using ^{13}C NMR where the carbons bonded to ^{18}O slightly shifts the signal upfield,[15] and Brown and Sy showed the changes of the deuterium signal in deuterium NMR spectroscopy[12] by monitoring a deuterated DHAA probe, which was injected through the roots of the dead plant, *Artemisia annua*. Furthermore, studies employing mass spectrometry to explore the endoperoxide forming mechanism are even more scarce.[16]

In particular, we previously reported the rate of spontaneous endoperoxide formation from [3,3-$^2H_2$]-dihydroartemisinic acid (3,3-d_2-DHAA, **3**) to artemisinin.[16] This cascade transformation occurred when dried down samples of 3,3-d_2-DHAA were left in vials open to air. Subsequently, liquid chromatography high-resolution mass spectrometry (LC-HRMS) was employed to quantify this spontaneous process (Figure 2, **3** to **6**, **2**, and **10**).[16] The rate of 3,3-d_2-artemisinin (**6**) formation from 3,3-d_2-DHAA (**3**) was determined to be faster in the presence of light. Additionally, an alternative mechanism was found to

Received: March 23, 2021
Published: June 17, 2021

https://doi.org/10.1021/acs.jnatprod.1c00246
J. Nat. Prod. 2021, 84, 1967−1984

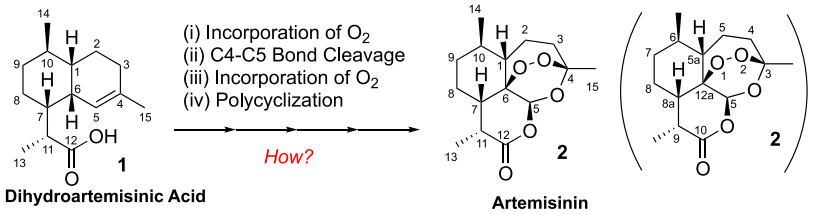

Figure 1. DHAA (**1**) is the biosynthetic precursor that converts to artemisinin (**2**). The structure of **2** shown in the figure has the carbons numbered in the same manner as **1** for clarity. The structure of **2** in parentheses shows the official numbering of the atoms in artemisinin.

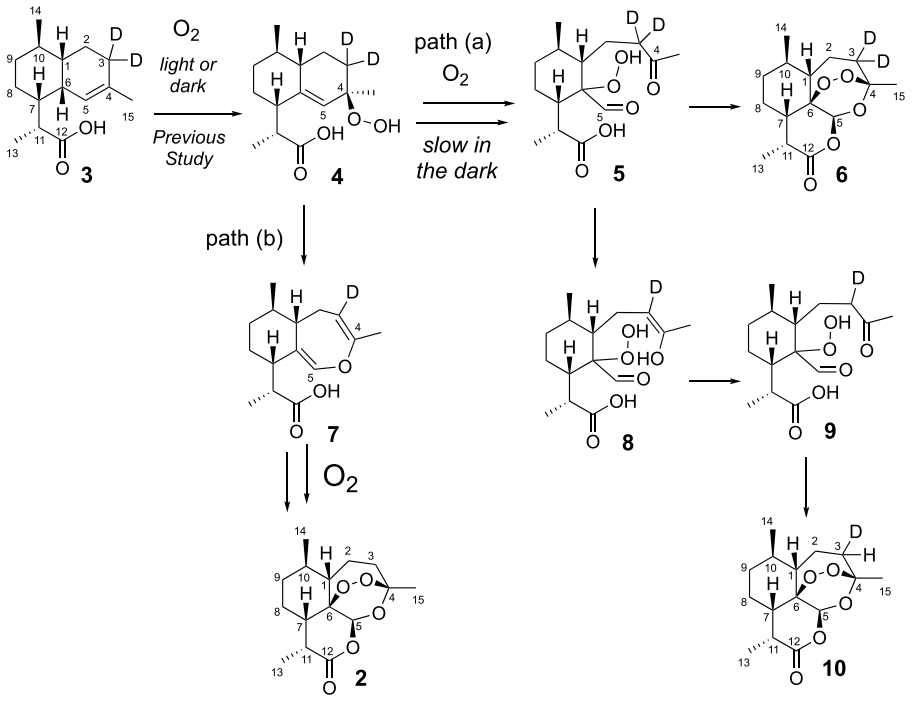

Figure 2. In the previous study,[16] 3,3-d_2-DHAA (**3**) was converted to a mixture of 3-d_1-artemisinin and 3,3-d_2-artemisinin isotopologues (**10** and **6**) through proposed path a, and nondeuterated artemisinin was converted through path b. In the presence of light, path a is dominant.

be operative with the detection of nondeuterated artemisinin (**2**) from 3,3-d_2-DHAA, which proceeded independent of light (path b of Figure 2).

The possibility of multiple mechanisms operating in the formation of artemisinin from DHAA (Figure 2) provided the inspiration to devise more experiments to elucidate the possible pathways of how this complex cascade reaction occurs.

The detection of nondeuterated artemisinin (**2**) from 3,3-d_2-DHAA (**3**) suggested an alternative pathway to endoperoxide formation involving a regioselective loss of the two C3 deuterium atoms in the formation of artemisinin (path b, Figure 2). Therefore, it was reasonable to synthesize [15,15,15-$^2H_3$]-dihydroartemisinic acid (15,15,15-d_3-DHAA, **11**) to mechanistically determine whether the C15 deuterium atoms would also be lost in its conversion to artemisinin with and without light (Figure 3, **11** to **16**, **17**, or **2**). Moreover, a completely trideuterated artemisinin isotopologue (**14**) could be potentially useful as an internal standard to quantify the conversion of nondeuterated DHAA to artemisinin (**1** to **2**).

This study involved the synthesis of 15,15,15-d_3-DHAA (**11**) and its use to investigate the mechanism of conversion of DHAA to artemisinin. Endoperoxide formation was tested under various conditions. In addition, the use of 3,3-d_2-DHAA (**3**) was revisited under these various conditions (Supporting Information). The formation of artemisinin was detected using liquid chromatography high-resolution mass spectrometry (LC-HRMS).

RESULTS AND DISCUSSION

(i) Synthesis of 15,15,15-d_3-DHAA (11). In order to deuterate the C15 position of DHAA (**1**), initial attempts involved the regioselective oxidation of **1** to obtain a C15-oxygenated intermediate (see Supporting Information, Part 12). However, all attempted routes to directly oxidize the C15-allylic methyl of the dehydrodecalin system had failed. Therefore, the synthesis of 15,15,15-d_3-DHAA (**11**) involved the cleavage of the C4−C5 bond (Figure 4, **1** to **21**) to enable the formation of a methyl ketone intermediate, which could be oxidized at the α-methyl position. The key deuterium incorporation step would employ the reaction of an α,β-unsaturated carbonyl intermediate (**18**) with $LiAlD_4$ and $AlCl_3$.[16] The C15-oxygenated intermediate would be derived from a Grubbs ring-closing metathesis (RCM) reaction of a monocyclic diene precursor (**19**). A Grubbs RCM has been previously employed to access the cis-dehydrodecalin system of DHAA.[17] Diene **19** would be derived from a silyl enol ether precursor (**20**). The key C15-oxygen would be incorporated through Rubottom oxidation of silyl enol ether **20**. The silyl enol ether would be accessed from the ketoaldehyde precursor (**21**) through olefination at C5 through a Wittig reaction. The ketoaldehyde intermediate

https://doi.org/10.1021/acs.jnatprod.1c00246
J. Nat. Prod. 2021, 84, 1967−1984

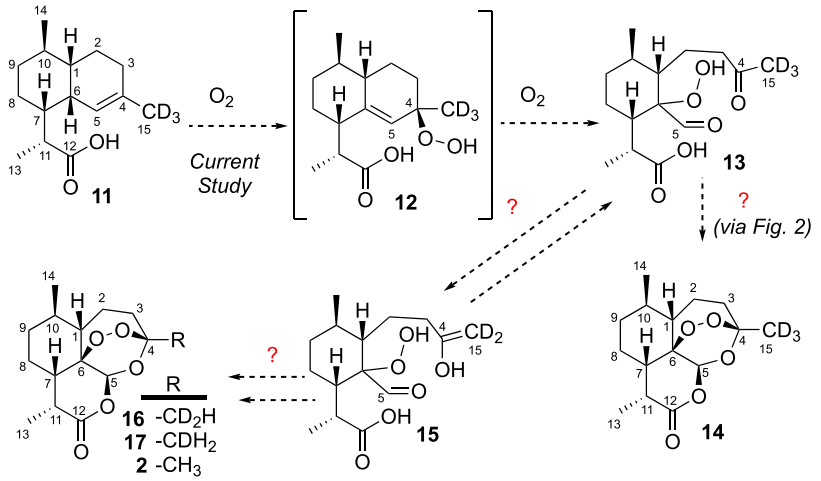

Figure 3. Regioselectively deuterated compound, 15,15,15-d_3-DHAA, was synthesized to determine whether any of the C15 deuterium atoms would be lost during its spontaneous conversion to artemisinin (**16**, **17**, or **2**).

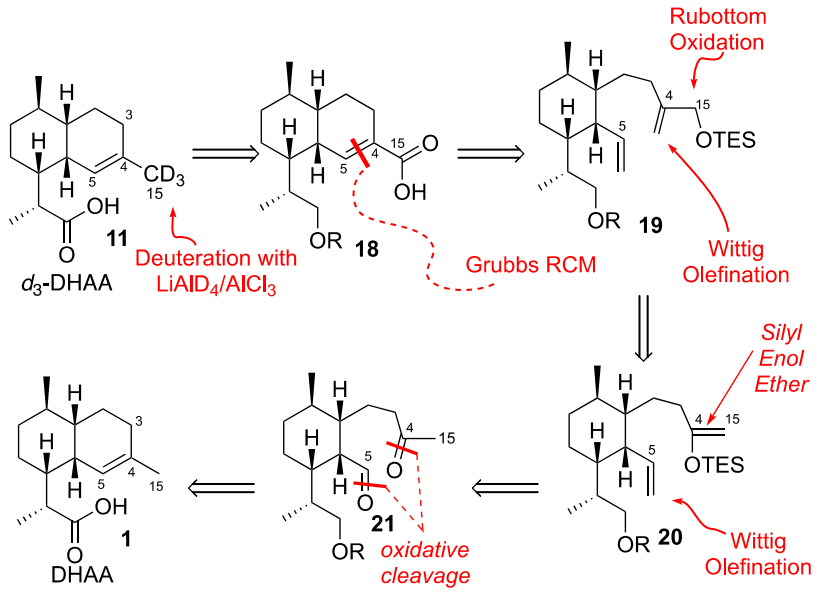

Figure 4. Retrosynthetic analysis of 15,15,15-d_3-DHAA (**11**) from DHAA (**1**).

(**21**) would in turn be derived through oxidative cleavage of the C4−C5 double bond of the cis-dehydrodecalin ring of DHAA (**1**).

DHAA (**1**) was treated with $NaIO_4$ in the presence of a catalytic amount of $RuCl_3$ and H_2SO_4 to dihydroxylate the C4−C5 bond and subsequently yield lactone **22** (Scheme 1). The resulting lactone **22** was reduced to triol **23** with $LiAlH_4$. Both lactone **22** and triol **23** were crystallized, and the stereochemistry was determined to be (4*R*, 5*S*) (Figure 5). Triol **23** was subsequently treated with $NaIO_4$ to cleave the C4−C5 bond to give lactol **24**. The resulting lactol was converted to TBDMS-protected primary ether **25**. The resulting ketoaldehyde **25** was reduced to diol **26** with $LiAlH_4$. A strong reducing agent such as $LiAlH_4$ was required for reduction, because when weaker hydride sources such as $NaBH_4$ were used, the reduction would stall at the lactol stage (data not shown). The C4-stereocenter was carried forward as an epimeric mixture (44/56 ratio determined by integrating the multiplets at δ 3.88 and 3.80, respectively) in the following six steps until this chiral center was oxidized to ketone **33**.

The primary alcohol of diol **26** was regioselectively protected as acetate **27** with acetyl chloride and triethylamine in CH_2Cl_2. The epimeric mixture at C4 remained unchanged; the ratio was determined to be 54/46 through integration of the two acetate methyl protons at δ 2.02 and 2.03. The resulting secondary alcohol of acetate **27** was protected as the TES ether **28** (56/44 epimeric mixture was determined by integrating the two multiplets at δ 3.78 and 3.72, respectively). The acetate was subsequently deprotected with MeLi to yield primary alcohol **29**. The C4 epimeric mixture was determined to be 52/48 by integrating the C14 methyl doublets at δ 0.86 and 0.84, respectively. The resulting alcohol was treated with Dess Martin periodinane (DMP) to yield aldehyde **30**, which was isolated as an epimeric mixture at C4 (56/44 determined by integrating the C4 methine protons at δ 3.76 and 3.69, respectively). Wittig olefination gave the monoalkene product **31** (51/49 epimeric mixture at C4 determined by integrating the C15 methyl protons at δ 1.13 and 1.12, respectively). Mild deprotection of the TES group with PPTS in MeOH afforded secondary alcohol **32**, which was determined to be a

https://doi.org/10.1021/acs.jnatprod.1c00246
J. Nat. Prod. 2021, 84, 1967−1984

Scheme 1. Synthesis of the Diene Intermediate 37 from DHAA (1)[a]

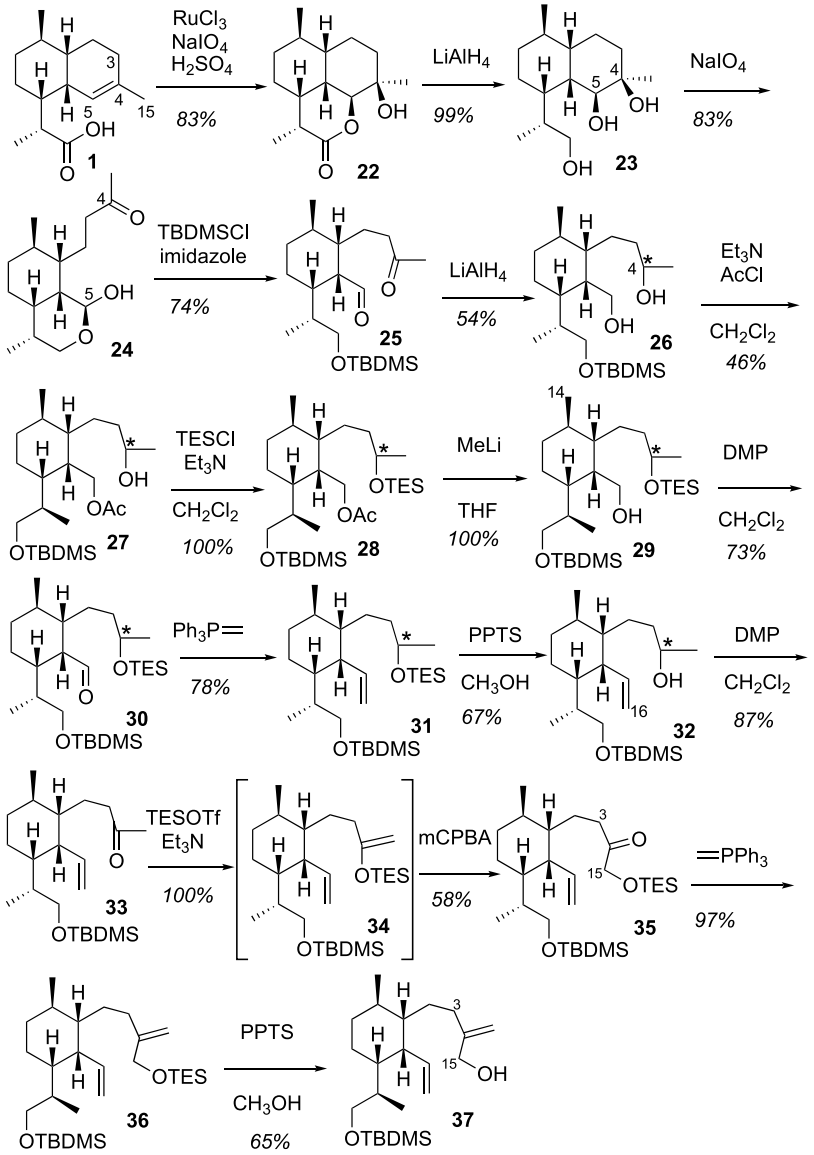

[a]* = carried forward from compound **26** as a diastereomeric mixture at C4 until the chiral center was converted to the ketone in compound **33**. The epimeric ratios of compounds **26**–**32** are described in the main text.

51/49 epimeric mixture at C4 through integrating the C16 alkene carbon signals at δ 117.4 and 117.5, respectively. The secondary alcohol was oxidized to methyl ketone **33** with DMP. TES triflate was used to convert methyl ketone **33** to the silyl enol ether derivative **34**. Silyl enol ether **34** was used as the crude material for the next step; careful inspection of the ^{1}H NMR spectrum indicated some of the undesired regioisomer (see Part 10 of the Supporting Information). Of the mixture, 28% was the more substituted silyl enol ether, while 72% was the desired silyl enol ether **34**. Rubottom oxidation of TES enol ether **34** with mCPBA incorporated the oxygen to yield α-substituted ketone **35**. Due to the mixture of silyl enol ether regioisomers, the undesired Rubottom oxidation product where the oxygen was incorporated at C3 was also incorporated. By integration of the corresponding protons, this ratio of the desired to undesired regioisomers was 81 to 19 (see Supporting Information for details). The ketone was converted to diene **36** upon treatment with methylenetriphenylphosphorane, to yield a regioisomeric mixture of 66 to 34; the major regioisomer was the desired diene **36**. The TES group of diene **36** was cleaved with PPTS in MeOH to yield allylic alcohol **37**. This deprotection to free alcohol **37** enabled the separation of the minor amount of the C3-alcohol through flash column chromatography. Details of this synthesis are included in the Supporting Information file.

With the key diene intermediate **37**, treatment with Grubbs second generation catalyst followed to give the cis-dehydrodecalin ring system (**38**) with the desired oxygen incorporated at C15 (Scheme 2). The allylic alcohol was oxidized with Dess Martin periodinane to yield the aldehyde intermediate (**39**). The aldehyde intermediate underwent Pinnick oxidation conditions to yield the carboxylic acid at C15 (**40**), which would be ready for deuterium incorporation. When the C15-carboxylic acid (**40**) was treated with $LiAlD_4$ and $AlCl_3$,[16] the dideutero alcohol was obtained (**41**) instead of the desired trideuteromethyl group. The yield of this reduction was 52% on a 70 mg scale. Therefore, only $LiAlD_4$ was used to reduce the carboxylic acid (**40**) to give the dideuterated alcohol intermediate

https://doi.org/10.1021/acs.jnatprod.1c00246
J. Nat. Prod. 2021, 84, 1967−1984

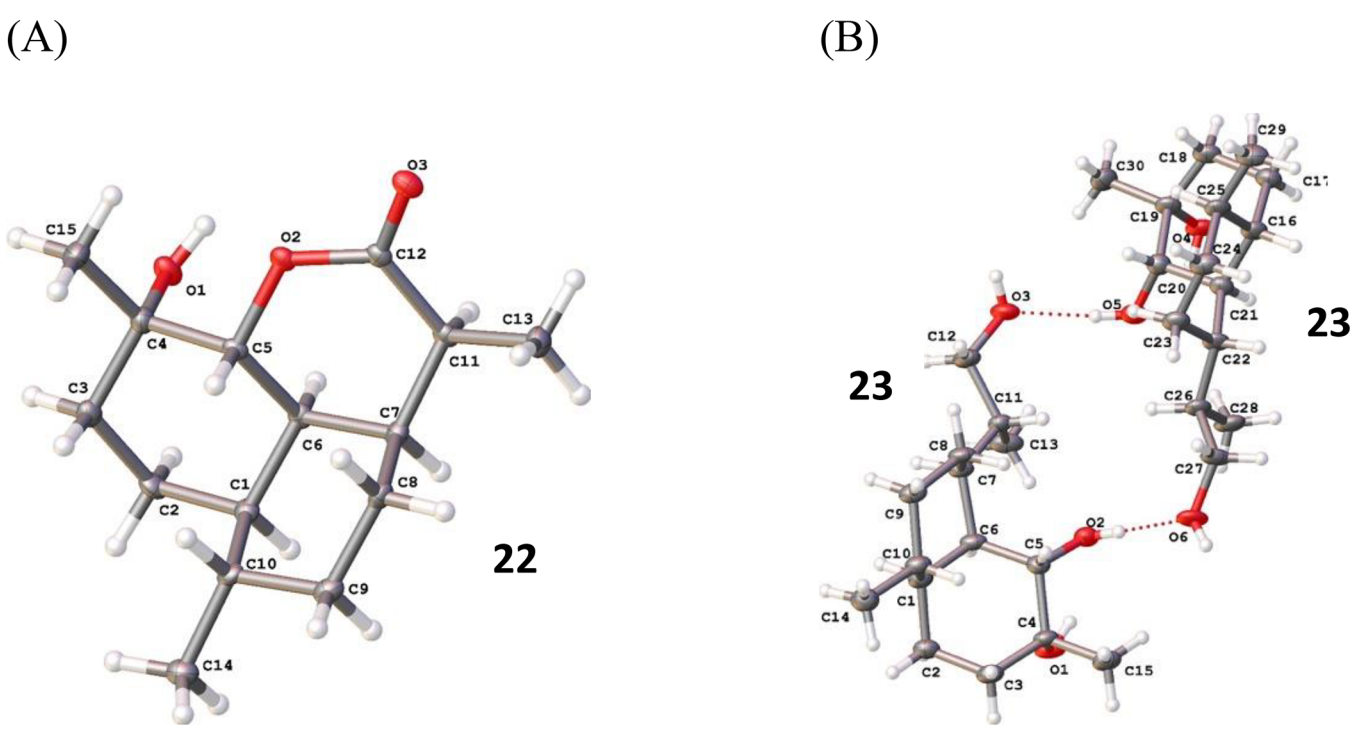

Figure 5. Crystal structures of (A) **22** and (B) **23**.

Scheme 2. Synthesis of 15,15,15-d_3-DHAA (11) from Diene Intermediate 37

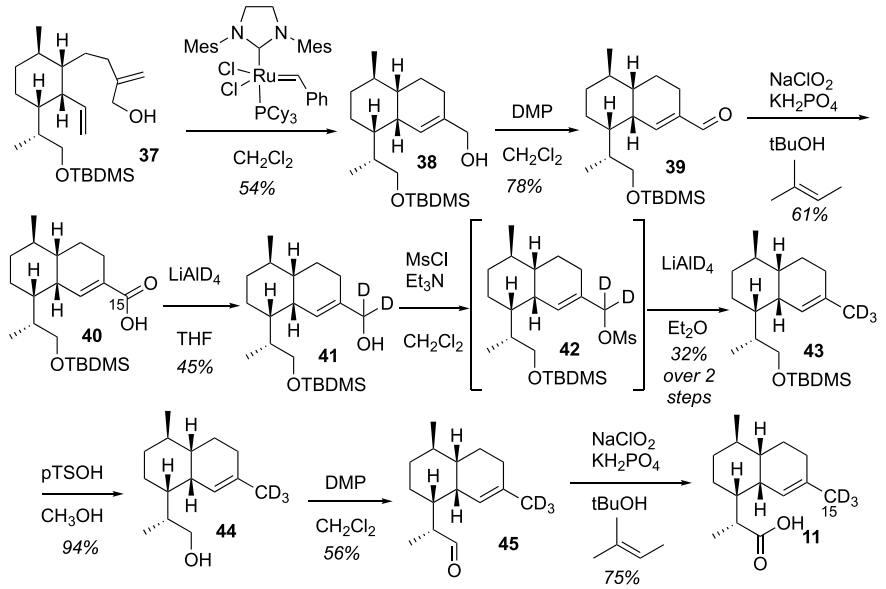

(**41**) in a 45% yield. The alcohol (**41**) was converted to mesylate **42** with methanesulfonyl chloride in the presence of stoichiometric amounts of Et_3N. Subsequent treatment of crude mesylate **42** with $LiAlD_4$ gave the desired trideuteromethyl intermediate (**43**) with a yield of 32% over two steps. The NMR spectrum of the crude reaction mixture showed the desired trideuteromethyl product **43** as the major product; therefore, the low yield is likely due to loss of material during the workup procedures for two steps. The TBDMS group of **43** was deprotected in the presence of stoichiometric amounts of pTsOH in CH_3OH to afford primary alcohol **44**. The final desired compound was obtained by treating primary alcohol **44** through the oxidation sequence of Dess Martin periodinane and Pinnick conditions to yield aldehyde **45** and 15,15,15-d_3-DHAA (**11**), respectively. The overall yield for the 25 steps to access 15,15,15-d_3-DHAA (**11**) from DHAA was 0.02% (Schemes 1 and 2).

(ii) Identification of UV-C Radiation to Promote the Conversion of DHAA to Artemisinin. In our previous study to determine the rate of the conversion of 3,3-d_2-DHAA to artemisinin (Figure 2, **3** to **6**), light was determined to accelerate the transformation.[16] However, in order to rule out heat as a factor to enhance the rate, several other conditions were tested to determine if heat were responsible in enhancing the rate of transformation of DHAA to artemisinin.

A solution of DHAA (**1**) in CH_2Cl_2 was aliquoted into three borosilicate glass vials; the solvent was evaporated by nitrogen flow, and each vial was left in different conditions: (1) in a

https://doi.org/10.1021/acs.jnatprod.1c00246
J. Nat. Prod. 2021, 84, 1967−1984

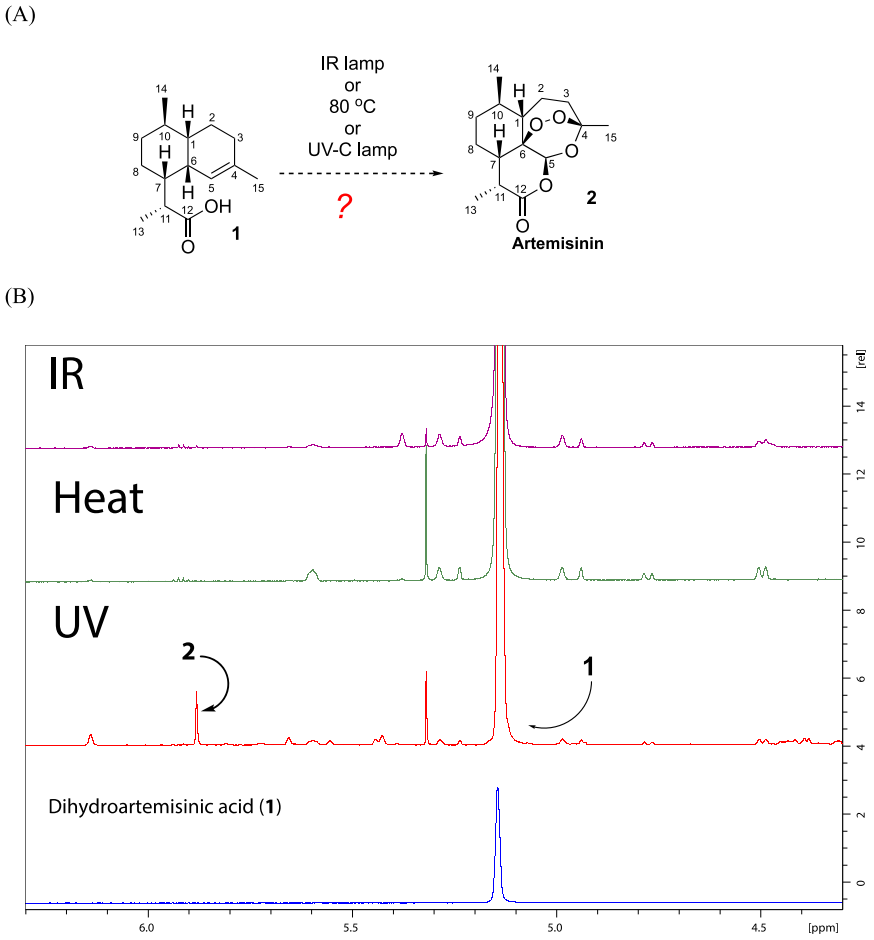

Figure 6. (A) Three conditions were tested to determine that UV-C light can enhance the rate of conversion of DHAA to artemisinin (**1** to **2**). (B) ^{1}H NMR spectroscopic overlay of the $CDCl_3$ extracts of the different conditions. Top spectrum = IR lamp at ambient temperature (purple), second row = heat at 80 °C (green), third row = UV-C light at ambient temperature (red), and bottom row = DHAA standard (blue). Both conditions with heat (IR lamp and 80 °C) produced less artemisinin (δ 5.88) compared to the conditions with a UV-C lamp within 2.5 h. ^{1}H NMR spectrum obtained on a 500 MHz NMR magnet in $CDCl_3$ solvent. Chemical shift range = δ 4.3−6.3.

box with an infrared (IR) lamp, (2) in a box with a UV-C lamp, and (3) in an oil bath in the fume hood set to 80 °C (Figure 6A). After 2.5 h, the contents of each vial were dissolved in $CDCl_3$, and ^{1}H NMR spectra were acquired. The results indicated that the UV-C lamp visibly formed artemisinin with the clear detection of artemisinin (the proton with δ 5.88 chemical shift), while the other two conditions (IR lamp and oil bath) had a smaller amount of artemisinin (Figure 6B). These results confirm that light, not heat, is responsible for enhancing the rate of conversion of DHAA to artemisinin. Notably, there are other chemical shifts present in all three conditions that are likely related to other products, but only the UV−C lamp conditions clearly resulted in the detection of artemisinin by ^{1}H NMR spectroscopy within 2.5 h (Figure 6B). There is a small signal that corresponds to artemisinin in the case of the IR radiation, but this signal is significantly smaller compared to the one found in the conditions involving UV-C irradiation.

(iii) Identification of a Light-Induced Rearrangement Product of Artemisinin. In order to identify a possible rearrangement pathway of artemisinin under UV-C light, a solution of artemisinin (**2**) in CH_2Cl_2 was dried down in a vial and placed under UV-C irradiation (Figure 7A). After 8 days under UV-C light, the material was purified, and a rearranged product that lacked the endoperoxide bridge was identified (**47**). The conversion of artemisinin to this rearranged product under UV-C irradiation suggests that, although light accelerates the conversion of DHAA to artemisinin (**1** to **2**), the exposure of light for too long will result in the conversion of artemisinin to this alternative rearranged product (Figure 7, **2** to **47**). The mechanism shows that, under UV-C light, the O−O bond of the endoperoxide homolytically cleaves and recombines to form the tetrahydrofuran ring, and the other oxygen radical recombines with the carbon radical to form the ester carbonyl. This rearranged product of artemisinin was also previously observed when artemisinin was heated to 190 °C.[18]

The presence of this rearranged product (**47**) was confirmed in plant extracts of *Artemisia annua* supplements and by matching the retention time and mass by LC-HRMS to the authentic standard (see Supporting Information, Part 5).

(iv) Time Course Studies with DHAA Isotopologues and Quantification with LC-HRMS. With the desired 15,15,15-d_3-DHAA isotopologue (**11**) in hand (*vide supra*), its conversion to artemisinin was measured through time course assays as previously developed with 3,3-d_2-DHAA[16] (Supporting Information (Part 7) and summarized in Table 1). In order to determine the effect of deuterium incorporation with respect to the rate of artemisinin formation, the rate of conversion of nondeuterated DHAA to artemisinin (**1** to **2**) was determined using a trideuterated artemisinin isotopologue

https://doi.org/10.1021/acs.jnatprod.1c00246
J. Nat. Prod. 2021, 84, 1967−1984

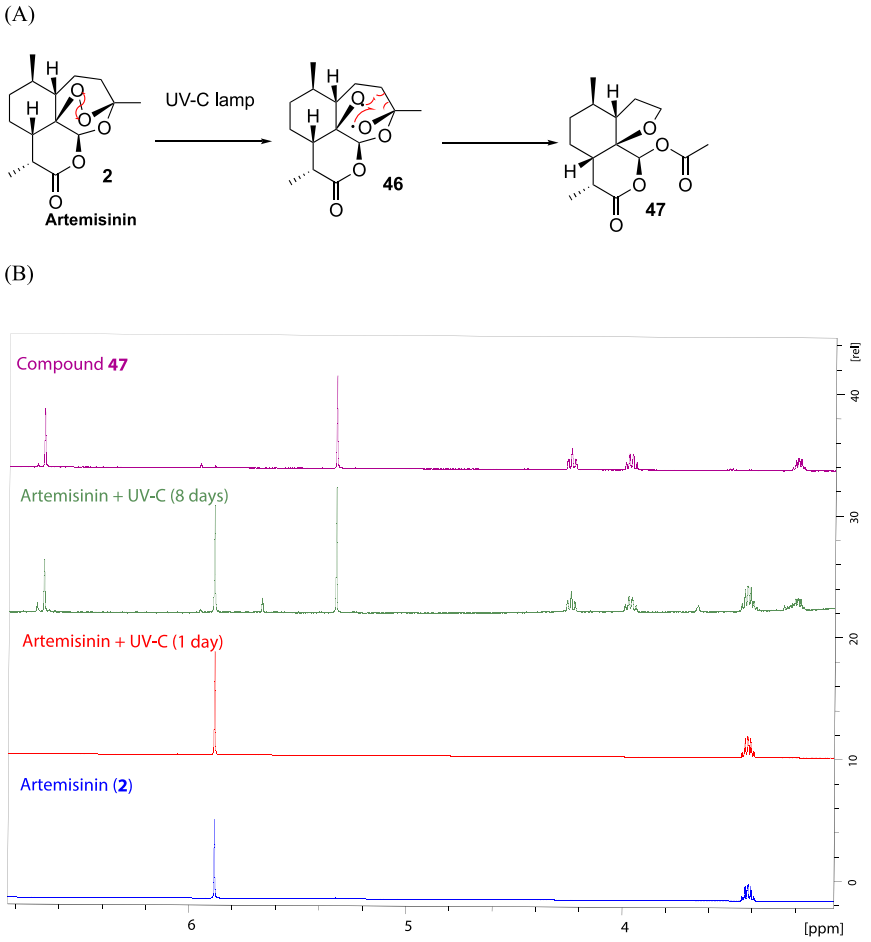

Figure 7. (A) Mechanism of light-induced rearrangement of artemisinin (**2** to **47**). (B) ^{1}H NMR spectroscopic overlay. Top = rearranged product. Second row = artemisinin exposed under UV-C lamp for 192 h (8 days). Third row = artemisinin exposed under UV-C lamp for 24 h. Bottom row = artemisinin standard. The singlet at δ 5.32 is CH_2Cl_2.

(**14**) as an internal standard. The influence of the density of DHAA on the rate was also determined by comparing the amount of artemisinin formed with a more dense and a less dense amount of DHAA (i.e., 100 and 10 μg of DHAA were used for Table 1 entries 1−12 and 13−24, respectively). In addition, three different conditions were tested that involved exposing DHAA to (i) ambient light, (ii) UV-C light (100−280 nm), and (iii) total darkness.

When 15,15,15-d_3-DHAA (**11**) was exposed to air in the dark and two sources of light, light by the window and a UV-C light source, d_3- and d_2-artemisinin isotopologues were predominantly formed (Figure 8). In our previous study with 3,3-d_2-DHAA (**3**), d_2-artemisinin (**6**) was formed at a 40-fold faster rate in the presence of light. It is important to note that the amount of light by the window may differ depending on the climate (i.e., the time of the year). In the previous study,[16] the window experiment was performed in May, while in the current study, the window experiment was performed in October when there is generally less sunlight. With 15,15,15-d_3-DHAA (**11**) as the starting material, d_3-artemisinin (**14**) was formed around 3-fold faster in the presence of ambient light at 24 and 47 h (Table 1). However, at 120 and 312 h, the rates of formation of artemisinin were almost equal in the presence and absence of light. The results of the time course are summarized in Table 1. At 24 h, the conditions that involved shining UV-C light to DHAA formed artemisinin the fastest (49-fold faster than conditions in the dark and 15-fold faster than conditions with ambient light). However, after 120 and 312 h, the conditions involving UV-C radiation resulted in less artemisinin detection compared to that of the conditions involving ambient light and dark conditions. This decrease in detection of artemisinin under UV-C irradiation at 120 h and beyond could be explained by the fact that, under UV-C irradiation, artemisinin begins to rearrange to the tetrahydrofuran product (Figure 7, *vide supra*). Indeed, the ion matching the calculated mass (m/z 331.2307) increasingly appears over time, especially under the UV-C conditions (see Supporting Information, Part 5). The same rearranged product is also observed by LC-HRMS when 3,3-d_2-DHAA (**3**) and DHAA (**1**) were used as the starting material under the UV-C irradiation conditions (see Supporting Information, Part 5). Figure 8B shows a representative LC-HRMS trace for the 120 h time point of 15,15,15-d_3-DHAA (**11**) in the presence of ambient light. Clearly, d_3-artemisinin (**14**) is the dominant isotopologue of artemisinin that is formed.

In order to test a density dependence on artemisinin formation from DHAA, similar time course experiments were performed but with less 15,15,15-d_3-DHAA (10 μg of **11**) in the vials (Supporting Information (Part 7), entries 13−24 in Table 1). The two types of samples had 100 and 10 μg of 15,15,15-d_3-DHAA (**11**) in each vial, respectively (see Supporting Information, Part 7). In general, the more dense samples of

https://doi.org/10.1021/acs.jnatprod.1c00246
J. Nat. Prod. 2021, 84, 1967−1984

Table 1. Results of Time Course Experiments of 15,15,15-d_3-DHAA (11) to d_3-Artemisinin (14)[a]

entry	condition	amount of 11	time	d_3-artemisinin (μg)	fold vs dark
1	light	100 μg	24 h	3.36×10^{-3}	3.3
2	light	100 μg	47 h	2.01×10^{-2}	3.5
3	light	100 μg	120 h	8.28×10^{-2}	1.2
4	light	100 μg	312 h	2.81×10^{-1}	1.1
5	dark	100 μg	24 h	1.01×10^{-3}	1.0
6	dark	100 μg	47 h	5.82×10^{-3}	1.0
7	dark	100 μg	120 h	6.78×10^{-2}	1.0
8	dark	100 μg	312 h	2.52×10^{-1}	1.0
9	UV-C	100 μg	24 h	4.94×10^{-2}	49
10	UV-C	100 μg	47 h	1.61×10^{-2}	28
11	UV-C	100 μg	120 h	1.14×10^{-2}	0.17
12	UV-C	100 μg	312 h	5.01×10^{-3}	0.020
13	light	10 μg	24 h	8.64×10^{-5}	5.6
14	light	10 μg	47 h	1.28×10^{-3}	Not Available
15	light	10 μg	120 h	7.49×10^{-3}	1.5
16	light	10 μg	312 h	1.89×10^{-2}	0.73
17	dark	10 μg	24 h	1.55×10^{-5}	1.0
18	dark	10 μg	47 h	Not Detected[b]	Not Available
19	dark	10 μg	120 h	4.97×10^{-3}	1.0
20	dark	10 μg	312 h	2.59×10^{-2}	1.0
21	UV-C	10 μg	24 h	6.63×10^{-3}	430
22	UV-C	10 μg	47 h	2.95×10^{-3}	Not Available
23	UV-C	10 μg	120 h	2.03×10^{-3}	0.41
24	UV-C	10 μg	312 h	3.83×10^{-3}	0.15

[a]Amount of d_3-artemisinin (14) formed from 15,15,15-d_3-DHAA (11) (either 100 or 10 μg in the vial). [b]The peak was not detected = the internal standard peak area (m/z 283 for d_0-artemisinin) was also relatively smaller than the other measurements (40 000 000 vs 110 000 000).

15,15,15-d_3-DHAA (100 μg of **11** in each vial) converted to d_3-artemisinin (**14**) at a faster rate. For instance, at 24 h in the presence of ambient light, 3.36 ng of d_3-artemisinin (**14**) formed in the more dense case, while only 86.4 pg of d_3-artemisinin (**14**) was formed when there was less DHAA in the vials, a 39-fold difference in formation of artemisinin.

Because more artemisinin is formed when the amount of DHAA is increased in the vials (100 vs 10 μg, Table 1), we propose possible intermolecular interactions between one DHAA molecule and a second DHAA molecule that initiates the endoperoxide forming cascade reaction (Figure 9). Moreover, when the C15-carboxylic acid is reduced to the alcohol, this alcohol is stable over time (i.e., there is no spontaneous endoperoxide formation), confirming a role for the carboxylic acid functional group[14] in DHAA to initiate the transformation to artemisinin. In order to further elaborate on the findings that increased amounts of DHAA results in an enhanced rate of endoperoxide formation, another set of experiments was performed to identify optimal conditions to convert DHAA to artemisinin (see Supporting Information, Part 14). Among the conditions, the addition of stoichiometric amounts of benzoic acid resulted in an enhanced rate of endoperoxide formation. The role of the carboxylic acid in enhancing endoperoxide formation is not completely clear, but a possible explanation is that the carboxylic acid provides the protons to promote polycyclization as shown in Figures 13, 16, and 17 (e.g., Figure 16, **64** to **65**).

In analyzing the amounts of artemisinin formed from 15,15,15-d_3-DHAA (**14** from **11**) in the presence and absence of light over time, the relative amounts of artemisinin differed considerably in the earlier time points (i.e., Table 1, 24 and 47 h). For instance, at 24 and 47 h, artemisinin was formed ∼3-fold faster in the presence of ambient light compared to in the absence of light (Table 1). However, at 120 and 312 h, the amount of artemisinin detected was ∼1.1- and ∼1.2-fold more in the presence of light. This observation could be explained by the fact that, over time, a layer of artemisinin forms on the surface of a lattice of DHAA and, in turn, blocks exposure of oxygen to the rest of DHAA (Supporting Information (Part 7), Figure S19). Another reason that the "dark" conditions form similar amounts of artemisinin compared to the "ambient light" at later time points (120 h and beyond) is, under the conditions involving light, artemisinin may be converting to the rearranged product (cf. Figure 7, **47**) over time. However, the rearranged product was not detected at the later time points (see Supporting Information, Part 5) by LC-HRMS probably because the mass spectrometer was not tuned for ionization to the rearranged product (instead, the instrument was tuned to detect artemisinin). Nonetheless, in our previous study,[16] when artemisinin was left under ambient light by the window for 64 days, the rearranged product was detected (see Supporting Information of reference). On the other hand, when the same amount of artemisinin was left in the dark for 64 days, no rearranged product was detected.

(v) Intermolecular Competitive Kinetic Isotope Effects. To expand on the observation of the rates of artemisinin formation from the different DHAA isotopologues and to determine the kinetic isotope effect (KIE), mixtures of the different DHAA isotopologues were made, and the artemisinin isotopologues were detected by LC-HRMS (Figures 10−12). When 15,15,15-d_3-DHAA (**11**) was mixed with nondeuterated DHAA (**1**) in a 1:1 ratio, nondeuterated DHAA converted to artemisinin at a faster rate (Figure 10). At all time points tested (48, 125, and 312 h), the C15-trideuterated DHAA isotopologue converted to artemisinin at a slower rate (Figure 10B). These rates were determined by measuring the amounts of d_3-artemisinin

https://doi.org/10.1021/acs.jnatprod.1c00246
J. Nat. Prod. 2021, 84, 1967−1984

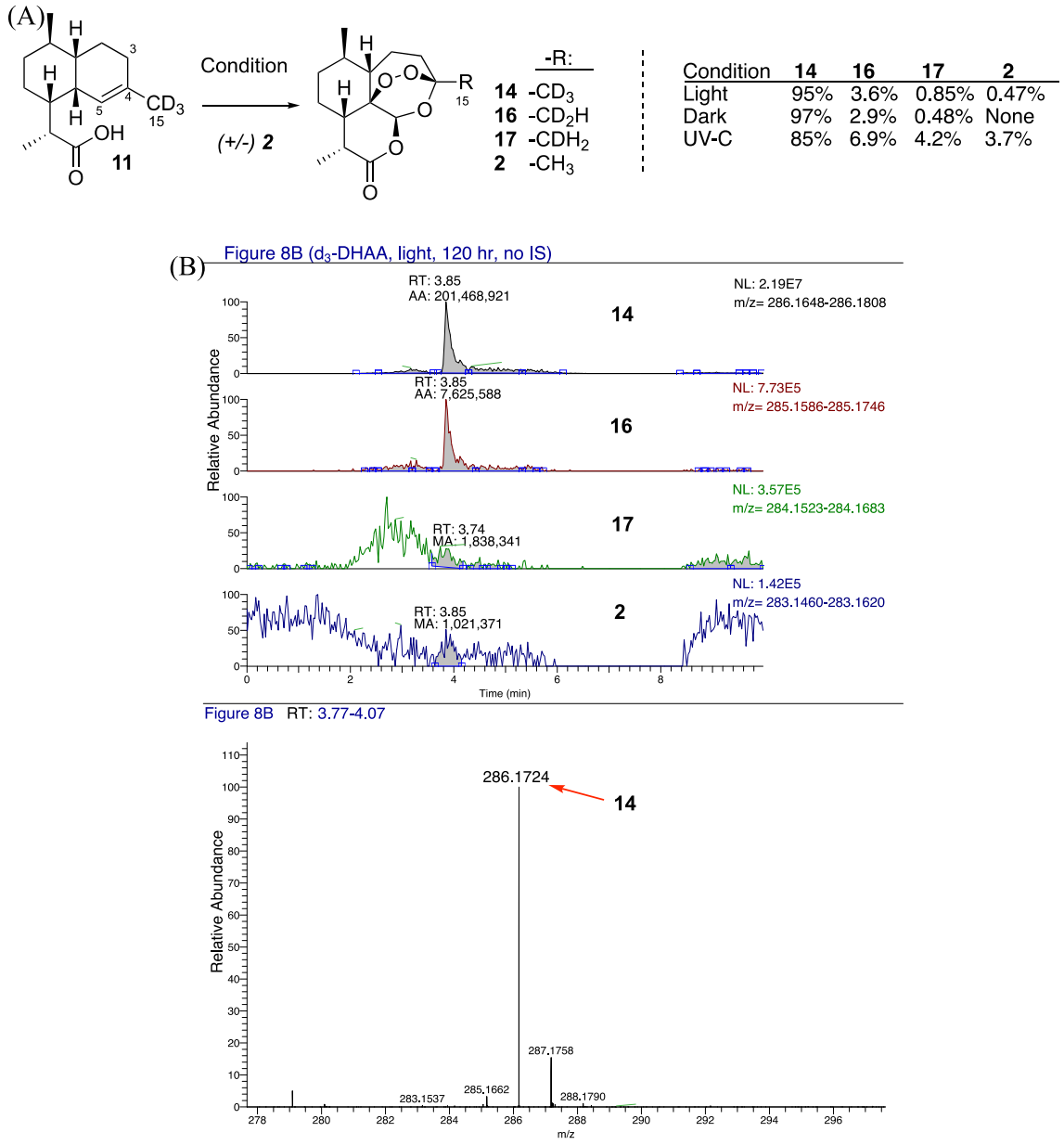

Figure 8. (A) Various conditions (i.e., ambient light, dark, UV-C, and different amounts of **11**) were tested to convert 15,15,15-d_3-DHAA (**11**) to artemisinin. Percentages indicate relative abundances of each artemisinin isotopologue at the 120 h time point (Supporting Information (Part 7) for LCMS traces). (B) Representative LCMS data for 120 h time point with ambient light (no internal standard). The data of the time course are summarized in Table 1.

and d_0-artemisinin by mass spectrometry (Supporting Information, Part 8).

Figure 11 shows the intermolecular kinetic isotope effect studies when DHAA was mixed in a 1:1 ratio with 3,3-d_2-DHAA (**3**). In all time points (48, 125, and 312 h), the nondeuterated version of DHAA converted to artemisinin at a faster rate compared to 3,3-d_2-DHAA (**3**) (Figure 11B). In summary, a kinetic isotope effect was observed in that nondeuterated DHAA (**1**) converted to artemisinin at a faster rate compared to the deuterated DHAA isotopologues (**3** and **11**). The KIE (k_H/k_D) values at C15 ranged from 2.23 to 3.31, while the KIE (k_H/k_D) values at C3 ranged from 2.05 to 2.42. The higher KIE values of d_3-DHAA could be associated with a secondary KIE.

On the other hand, Figure 12 shows the intermolecular competitive KIE experiments between 3,3-d_2-DHAA (**3**) and 15,15,15-d_3-DHAA (**11**) in the formation to artemisinin. At 48 and 125 h, the rates of artemisinin formation were similar, but at 312 h, 3,3-d_2-DHAA (**3**) converted to artemisinin at a faster rate (3-fold, see Figure 12B).

Based on the observed kinetic isotope effects from the different rates of conversion of DHAA isotopologues to artemisinin (Figures 10 and 11), the initial ene reaction between DHAA and one molecule of oxygen is proposed to occur via three different modes (Figure 13). Deuteration at either the C3 or the C15 position resulted in a slower rate of conversion to artemisinin from DHAA. Each resulting allylic hydroperoxide intermediate (Figure 13, **49**, **52**, and **55**) is eventually converted to the same oxonium (**53**) that reacts with a second molecule of oxygen to ultimately form artemisinin (**2**). The values for the intermolecular kinetic isotope effects ranging from 2.1 to 3.3

https://doi.org/10.1021/acs.jnatprod.1c00246
J. Nat. Prod. 2021, 84, 1967−1984

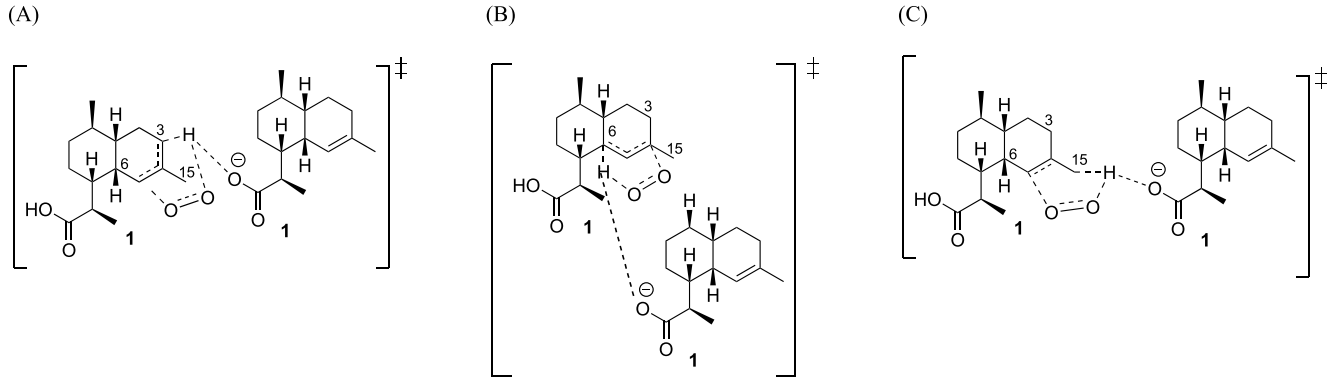

Figure 9. Alternative intermolecular interactions between DHAA (**1**) molecules proposed in promoting the different ene reactions shown in Figure 13. (A) The neighboring carboxylate interacts with the hydrogen at C3. (B) The neighboring carboxylate interacts with the hydrogen at C6. (C) The neighboring carboxylate interacts with the hydrogen at C15.

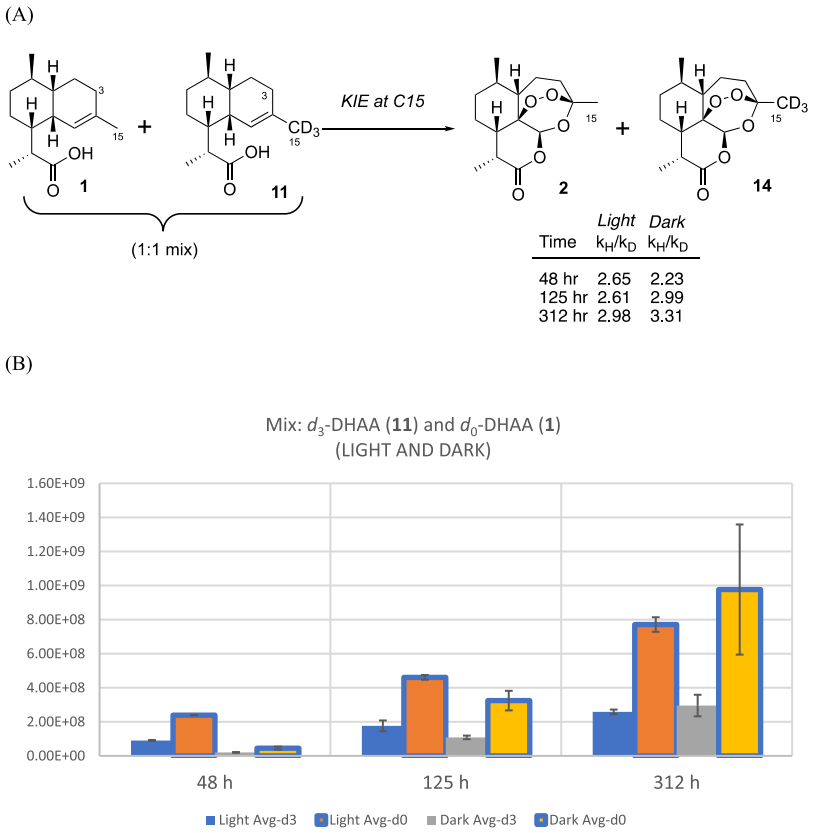

Figure 10. Kinetic isotope effect was directly measured by using a (A) 1:1 mixture of DHAA (**1**) and 15,15,15-d_3-DHAA (**11**). The artemisinin isotopologues (**2** and **14**) were detected by LC-HRMS at 48, 125, and 312 h. (B) Chart summarizing the results. For Figures 10−12, see Supporting Information (Parts 8 and 11) for LC-HRMS traces. The bars on the chart in (B) are the standard deviation values of two different data points. *y*-axis = areas of the artemisinin isotopologues.

(Figures 10 and 11) are reasonable when compared to a previous study of a nitrosoarene ene reaction[19] (k_H/k_D ~2).

Alternative to the concerted ene reactions shown in Figure 13, the formation of the allylic hydroperoxides can be rationalized through a perepoxide (Figure 14, **57**).[20] However, in the case of the mechanism through a perepoxide intermediate, the formation of the perepoxide is the rate-limiting step, and subsequent rearrangement is fast. Therefore, through this particular mechanism, when singlet oxygen undergoes an ene reaction, intermolecular kinetic isotope effect values for the ene reaction are usually smaller[21] (k_H/k_D ~ 1.0 and 1.1). Similarly, a biradical mechanism[22] can also be ruled out due to the high-energy state of a biradical intermediate compared to the lower barrier for hydrogen atom abstraction, which would result in a small kinetic isotope effect (k_H/k_D ~1−2).

(vi) $^{18}O_2$ Labeling Studies for Endoperoxide Formation from DHAA. In order to test the oxygen incorporation mechanism to form the endoperoxide from DHAA, $^{18}O_2$ (99%, ^{18}O) was used in the presence of 15,15,15-d_3-DHAA (**11**) (Figure 15). Although a previous study had determined a mixture of ^{18}O incorporation when DHAA hydroperoxide was exposed to $^{18}O_2$,[15] there has not been a previous study that performed the $^{18}O_2$ experiment from DHAA. Surprisingly, ^{18}O was incorporated into artemisinin from DHAA, but

https://doi.org/10.1021/acs.jnatprod.1c00246
J. Nat. Prod. 2021, 84, 1967−1984

(A)

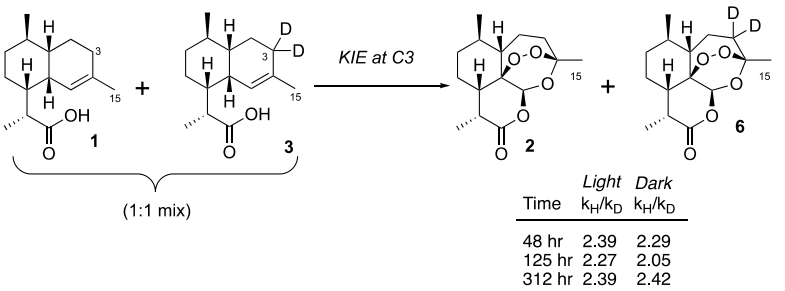

(B)

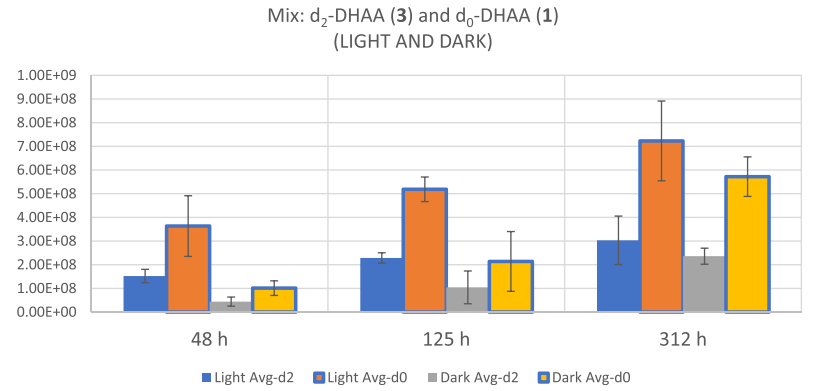

Figure 11. (A) Kinetic isotope effect was directly measured by using a 1:1 mixture of DHAA (**1**) and 3,3-d_2-DHAA (**3**). The artemisinin isotopologues (**2** and **6**) were detected by LC-HRMS at 48, 125, and 312 h. (B) Chart summarizing the results. *y*-axis = areas of the artemisinin isotopologues.

(A)

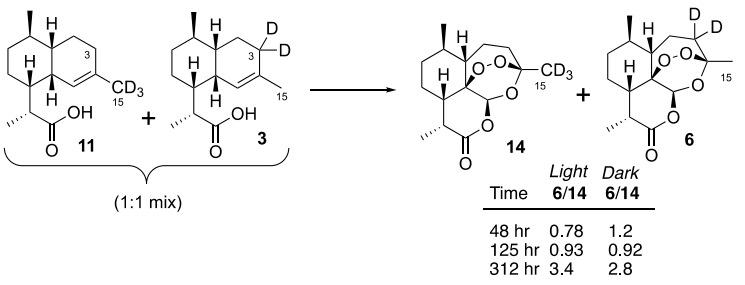

(B)

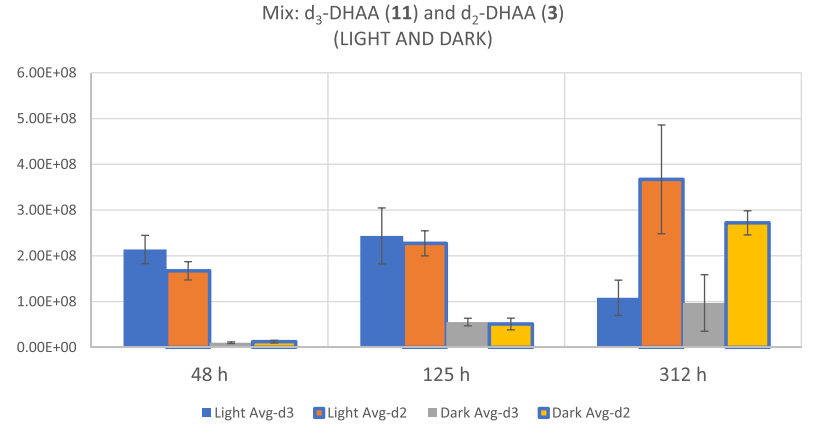

Figure 12. (A) The kinetic isotope effect was directly measured by using a 1:1 mixture of 15,15,15-d_3-DHAA (**11**) and 3,3-d_2-DHAA (**3**). The artemisinin isotopologues (**14** and **6**) were detected by LC-HRMS at 48, 125, and 312 h. (B) Chart summarizing the results. *y*-axis = areas of the artemisinin isotopologues.

https://doi.org/10.1021/acs.jnatprod.1c00246
J. Nat. Prod. 2021, 84, 1967−1984

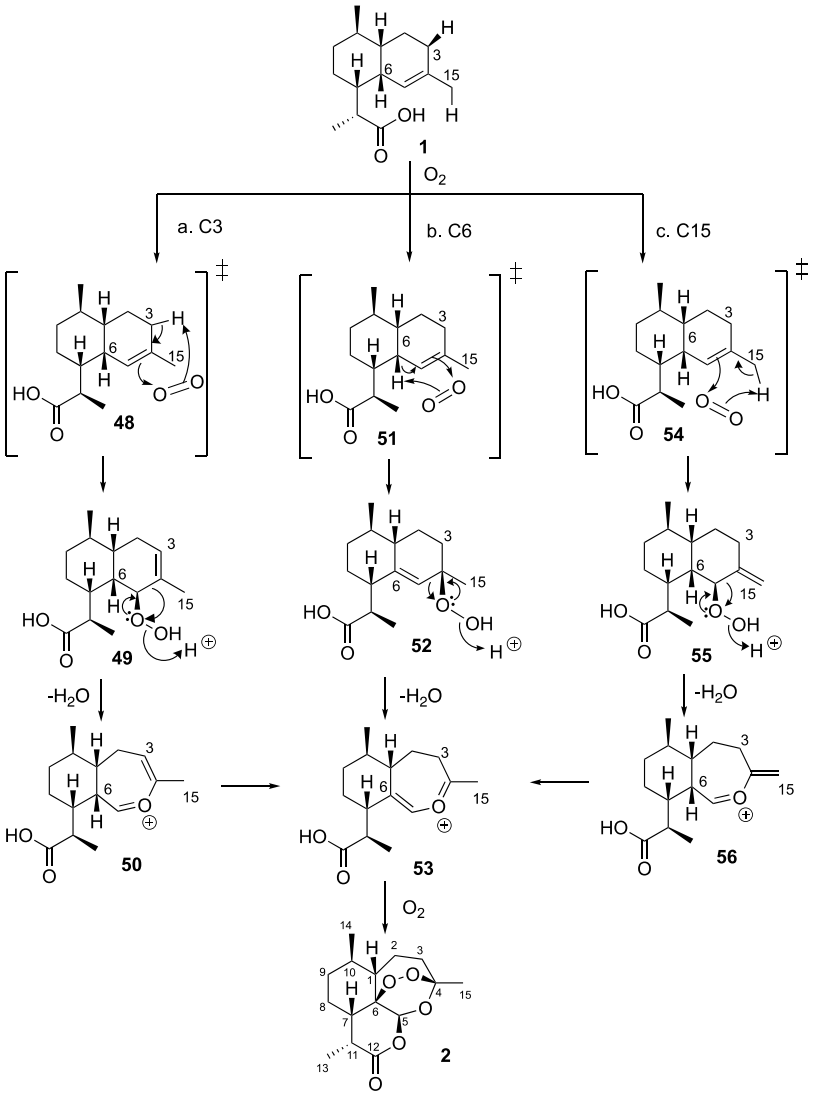

Figure 13. Three possible ene reactions (at C3, C6, or C15) are illustrated that involve the interaction of DHAA (**1**) with a molecule of oxygen. The resulting allylic hydroperoxides (**49**, **52**, and **55**) can converge to a common oxonium intermediate (**53**), which reacts with another molecule of O_2 to form artemisinin (**2**). A mechanism is proposed for the reaction with the second molecule of oxygen in Figure 16.

the isotopic composition was 1.0:7.2:14 for $^{18}O_2$:$^{18}O_3$:$^{18}O_4$ in the artemisinin product (Figure 15, Table 2: 71 h entry).

Two different time points were taken for the exposure of 15,15,15-d_3-DHAA (**11**) to $^{18}O_2$, 71 h and 14 days, to determine the effect of time and ^{18}O incorporation (Table 2). These experiments were performed in the presence of light (see Supporting Information, Part 9). Notably, at the longer time point (14 days), there was a significant amount of artemisinin with no ^{18}O atoms incorporated (see Supporting Information). This lack of ^{18}O incorporation suggests that the oxygen ($^{16}O_2$) from the atmosphere was permeating through the reaction vessel, which may not have been completely sealed from the environment. Nonetheless, this information was useful in that the amount of artemisinin that lacked ^{18}O atoms directly correlated with the amount of artemisinin with one and two ^{18}O atoms incorporated. Table 2 summarizes the results from the $^{18}O_2$ studies.

A mechanism to explain the mixture of isotopologues is shown in Figure 16. DHAA (**1**) undergoes an initial ene reaction, which can yield the oxonium intermediate (Figure 16, **63**). This initial ene reaction can go through multiple mechanistic pathways as shown above in Figure 13. The resulting oxonium (**63**) can be attacked either by ^{18}O labeled water to yield the cyclic hemiketal intermediate (**64**) through pathway a in Figure 16. The resulting hemiketal (**64**) can attack molecular oxygen ($^{18}O_2$) to yield the peroxide (**65**). This peroxide (**65**) can cyclize through intramolecular nucleophilic attack of the peroxide moiety onto the ketone, which subsequently attacks the aldehyde and cyclizes with the carboxylic acid to yield the endoperoxide with four ^{18}O atoms (**66**).

Alternatively, oxonium **63** can be attacked by the ^{16}O water (pathway b, Figure 16) to yield hemiketal **67**. This hemiketal can attack $^{18}O_2$ to yield the peroxide (**68**). The oxonium **68** can undergo intramolecular nucleophilic attack by the carboxylic acid to yield the lactone (**69**). The hemiketal of **69** could dehydrate to yield the oxonium **70** (pathway c, Figure 16), which undergoes cyclization to yield artemisinin with three ^{18}O atoms (**71**).

In a third pathway from intermediate **69**, the hemiketal could open to yield ketone **72** (pathway d in Figure 16). The resulting hemiacetal (**72**) could dehydrate to yield oxonium **73**, which could undergo polycyclization to yield the artemisinin

https://doi.org/10.1021/acs.jnatprod.1c00246
J. Nat. Prod. 2021, 84, 1967−1984

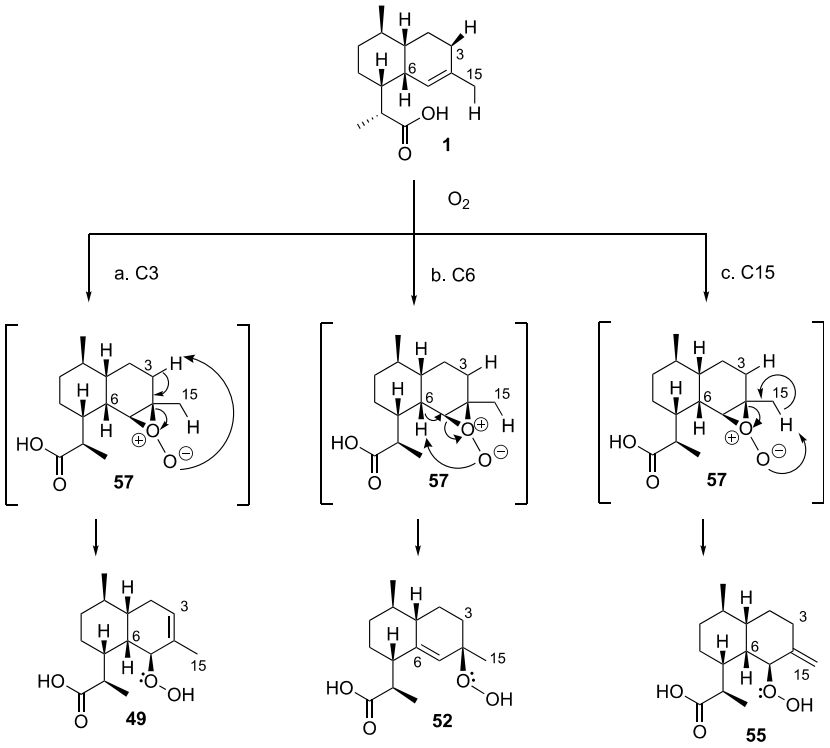

Figure 14. Alternative stepwise mechanism for the ene reaction to convert DHAA (**1**) to the different allylic hydroperoxide intermediates (**49**, **52**, and **55**) from perepoxide **57**.

isotopologue with two ^{18}O atoms (**75**). Table 2 summarizes the different ratio of artemisinin isotopologues produced from the exposure of 15,15,15-d_3-DHAA (**11**) to $^{18}O_2$.

An alternative to the pathway presented in Figure 16 to obtain artemisinin with three ^{18}O atoms (compound **71**) is presented in Figure 17. The carboxylic acid intermediate **65** could potentially undergo a cyclization process that is initiated by the carboxylic acid moiety nucleophilically attacking the aldehyde functional group to form the cyclic hemiacetal (**76**), which results in the loss of one of the ^{18}O atoms through a dehydration process (**76** to **77**). The resulting oxonium can undergo a cyclization to form artemisinin with three ^{18}O atoms incorporated (**77** to **71**). Other possible mechanisms are presented in the Supporting Information (Part 9, Figures S38 and S39).

CONCLUSION

In conclusion, a synthesis of 15,15,15-d_3-DHAA (**11**) was accomplished from DHAA (**1**). Subsequent conversion to artemisinin indicated artemisinin formation at a faster rate in the presence of UV-C radiation initially (Table 1, 24 h). However, at later time points (47, 120, and 312 h), more artemisinin was detected in the presence of ambient light and in darkness due to a rearrangement of artemisinin promoted by UV-C irradiation (Figure 7). A comparison of rates of artemisinin formation from 15,15,15-d_3-DHAA (**11**), 3,3-d_2-DHAA (**3**), and DHAA showed that nondeuterated DHAA converted to artemisinin the fastest (i.e., **1** to **2** was the fastest), indicating a kinetic isotope effect in the initial ene reaction with molecular oxygen (Figures 10 and 11, $k_H/k_D \sim 2.1-3.3$). This result supported multiple ene reactions that occur at the C3-, C6-, and C15-positions of DHAA (Figures 13 and 14). Furthermore, when 15,15,15-d_3-DHAA (**11**) was exposed to $^{18}O_2$ (99% ^{18}O) over time, a mixture of artemisinin isotopologues containing four and three ^{18}O atoms formed (Figure 15B and Table 2). These ^{18}O labeling experiments also confirm a mixed mechanism toward endoperoxide formation in the conversion of DHAA to artemisinin (Figures 16 and 17). Collectively, these results support a mixed mechanistic pathway when two molecules of oxygen react with DHAA to form the endoperoxide functional group (Figure 18). In addition, it is notable that UV-C light: (i) promotes the conversion of DHAA to artemisinin (Figure 18, **1** to **66** and **71**) and (ii) accelerates a rearrangement of the endoperoxide bridge of artemisinin to a tetrahydrofuran product (Figure 7, **2** to **47**, and Figure 18, **66** and **71** to **82**).

These observations are relevant in optimizing the light-driven process to convert DHAA to artemisinin where there should be enough to efficiently produce the endoperoxide bridge but not too much to prevent the rearrangement and loss of the endoperoxide.

EXPERIMENTAL SECTION

General Experimental Procedures. Melting points were recorded on a Global Medical and Lab Solutions melting point apparatus (India). A JASCO P-1010 polarimeter (JASCO Inc. Easton, MD) was used for measuring optical rotations of compounds. IR data were obtained on an FTIR instrument (Nicolet iS50 FT-IR spectrometer, Thermo Fisher Scientific, Waltham, MA, USA). The IR data were analyzed on OMNIC software (Thermo Fisher Scientific). A Bruker (Billerica, MA) 300 or 500 MHz NMR spectrometer was used to characterize compounds presented in the synthesis. NMR data were analyzed using either Topspin software (Bruker) or Mestrenova software (Mestrelab, Santiago de Compostela, A Coruña, Spain). $CDCl_3$ (Cambridge Isotope Laboratories, Tewksbury, MA) was used as the NMR solvent for the obtained spectra. The chloroform peaks for the proton and ^{13}C NMR spectra were referenced to δ 7.26 and δ 77.16, respectively. An LTQ Orbitrap XL mass spectrometer (Thermo) connected to an Acuity (Waters, Milford, MA) UPLC system was used to analyze compounds.

https://doi.org/10.1021/acs.jnatprod.1c00246
J. Nat. Prod. 2021, 84, 1967−1984

(A)

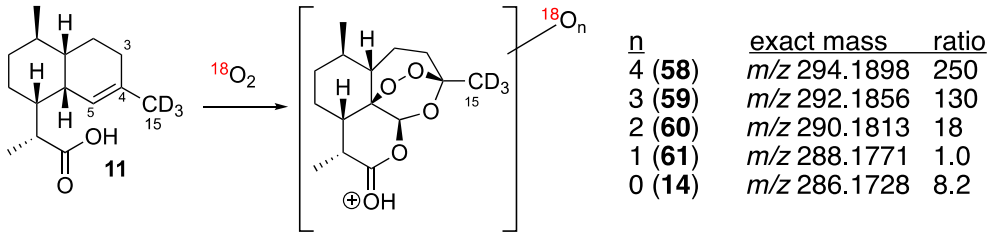

n	exact mass	ratio
4 (**58**)	*m/z* 294.1898	250
3 (**59**)	*m/z* 292.1856	130
2 (**60**)	*m/z* 290.1813	18
1 (**61**)	*m/z* 288.1771	1.0
0 (**14**)	*m/z* 286.1728	8.2

(B)

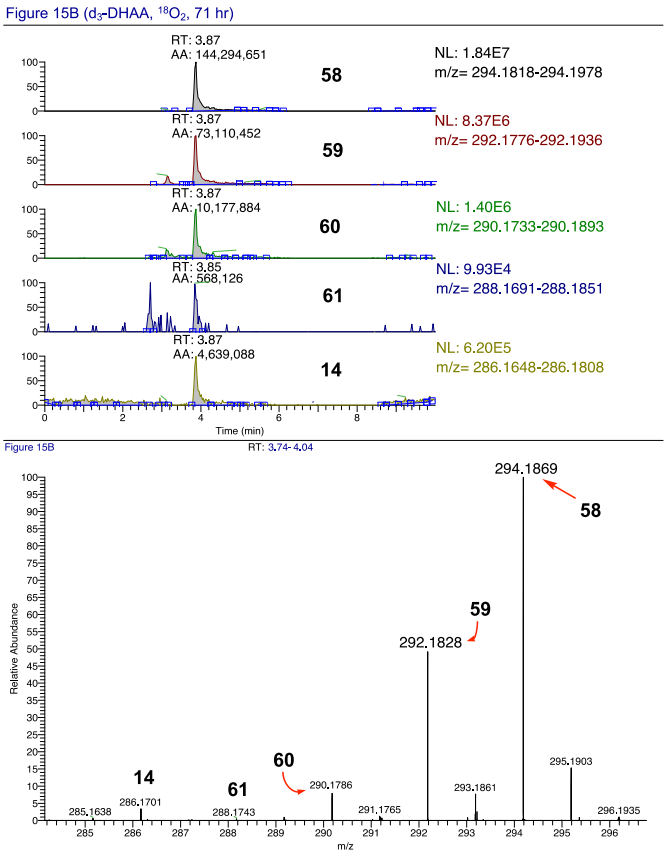

Figure 15. (A) Reaction of $^{18}O_2$ with 15,15,15-d_3-DHAA (**11**). LC-MS results for (B) 71 h with ambient light. A mechanism for ^{18}O incorporation from molecular oxygen ($^{18}O_2$) is proposed in Figure 18. Extracted ion chromatogram in (B) is shown with an 8 ppm mass tolerance window. *n* = number of ^{18}O atoms incorporated into artemisinin.

Xcalibur 2.1 software (Thermo Scientific) was used to analyze liquid chromatography mass spectrometry (LCMS) data. Prior to analysis, the mass spectrometer was calibrated with ESI positive mode or ESI negative mode solution (Thermo Scientific, Waltham, MA). $^{18}O_2$ gas (99% ^{18}O) was purchased from Sigma-Aldrich (St. Louis, MO). TLC plates (silica gel) with fluorescent indicator (254 nm) were used to analyze compounds. The compounds were visualized with CAM stain (Ceric Ammonium Molybdate recipe: 2.35 L of water, 120 g of ammonium molybdate, 5 g of ceric ammonium molybdate, and 150 mL of concentrated sulfuric acid). For time course studies with DHAA to artemisinin measurements, clear glass 2 mL screw cap vials were used for the light conditions, and amber glass 2 mL screw cap vials were used for the dark conditions.

X-ray Crystallography. *X-ray Crystal Data for 1.* Directly from the commercial source, **1** was obtained as colorless blocks. Crystallogrpahic data were collected at 100.0(1) K on a XtaLAB Synergy/Dualflex, HyPix fitted using Cu K_α, λ = 1.541 84 Å, followed by empirical absorption correction using spherical harmonics, implemented in SCALE3 ABSPACK[23] scaling algorithm. The structure was solved by direct methods (OLEX2[24] and ShelXT)[25] and refined against F^2 with full-matric least-squares using the program ShelXL.[26] All non-hydrogen atoms were refined with anisotropic displacement parameters. All H atoms, bound to carbon atoms, were placed on calculated positions and refined using the riding model with isotopic displacement parameters based on those of the parent atom. The oxygen bound hydrogen atom, H2, position was determined by electron density plot.

The crystallographic data can be obtained free of charge via https://www.ccdc.cam.ac.uk/structures/ or from the Cambridge Crystallographic Data Center, 12 Union Road, Cambridge CB2 1EZ, UK; fax: (+44)1223−336−033; or e-mail: deposit@ccdc.cam.ac.uk. CCDC number 2061809.

$C_{15}H_{24}O_2$, M = 236.34, 0.216 × 0.171 × 0.076 mm^3, orthorhombic, space group $P2_12_12_1$ (no. 19), a = 6.24107(9) Å, b = 8.21018(12) Å, c = 26.5277(5) Å, V = 1359.29(4) $Å^3$, Z = 4, D_c = 1.155 g cm^{-3}, μ = 0.580 mm^{-1}. F_{000} = 520, $2\theta_{max}$ = 152.4°,

https://doi.org/10.1021/acs.jnatprod.1c00246
J. Nat. Prod. 2021, 84, 1967−1984

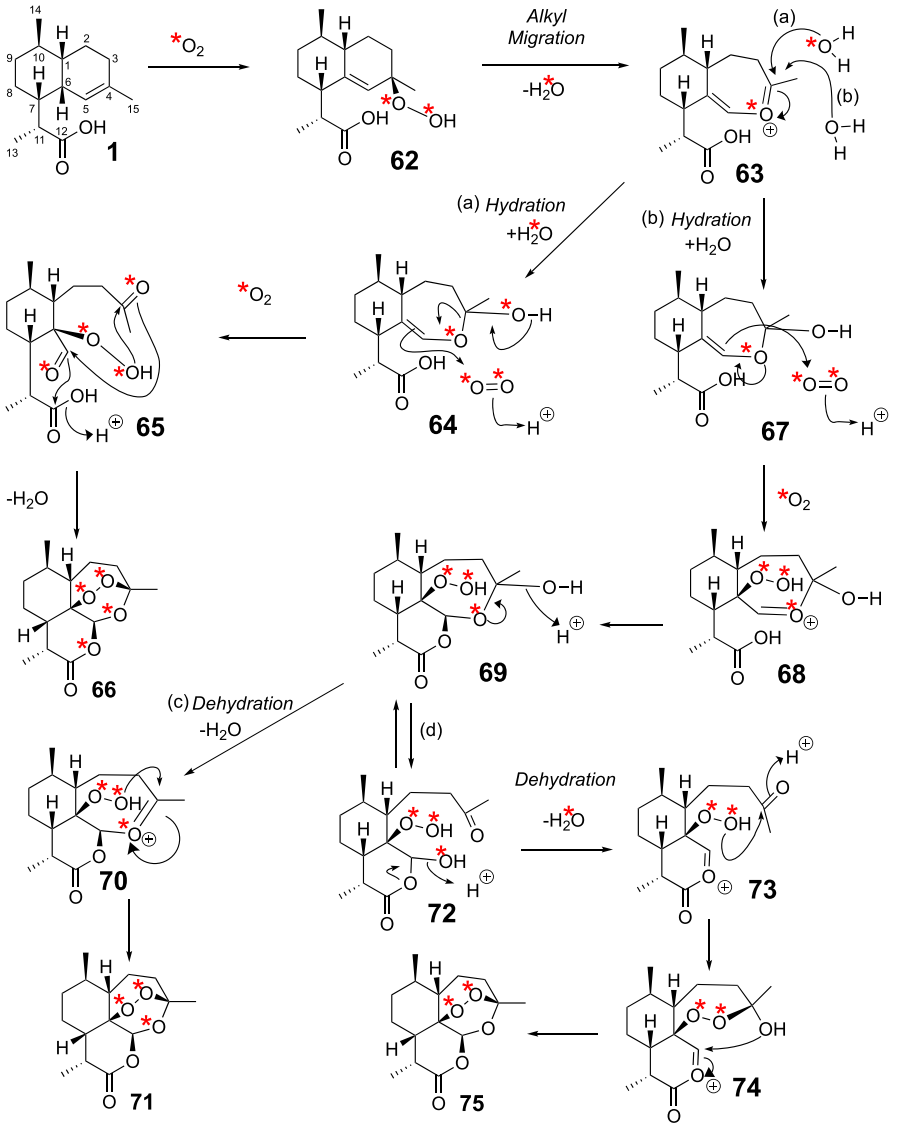

Figure 16. Proposed mechanism of oxygen incorporation into the endoperoxide bridge from DHAA (**1**) based on $^{18}O_2$ studies. *O = ^{18}O.

9206 reflections collected, 2578 unique (R_{int} = 0.0325). Final GOOF = 1.014, R_1 = 0.0304, wR_2 = 0.0780, R indices based on 2454 reflections with $I > 2\sigma(I)$ (refinement on F^2), $|\Delta\rho|_{max}$= 0.170 e Å^{-3}, 161 parameters, 0 restraints.

X-ray Crystal Data for ***2***. Directly from the commercial source, **2** was obtained as colorless blocks. Crystallogrpahic data were collected at 100.0(1) K on a XtaLAB Synergy/Dualflex, HyPix fitted using Cu K_α, λ = 1.541 84 Å, followed by empirical absorption correction using spherical harmonics, implemented in SCALE3 ABSPACK[23] scaling algorithm. The structure was solved by direct methods (OLEX2[24] and ShelXT)[25] and refined against F^2 with full-matric least-squares using the program ShelXL.[26] All non-hydrogen atoms were refined with anisotropic displacement parameters. All H atoms, bound to carbon atoms, were placed on calculated positions and refined using the riding model with isotopic displacement parameters based on those of the parent atom.

The crystallographic data can be obtained free of charge via https://www.ccdc.cam.ac.uk/structures/ or from the Cambridge Crystallographic Data Center, 12 Union Road, Cambridge CB2 1EZ, UK; fax: (+44)1223−336−033; or e-mail: deposit@ccdc.cam.ac.uk. CCDC number 2061808.

$C_{15}H_{22}O_5$, M = 282.32, 0.169 × 0.096 × 0.062 mm^3, orthorhombic, space group $P2_12_12_1$ (no. 19), a = 6.3116(2) Å, b = 23.9499(6) Å, c = 9.3103(3) Å, V = 1406.28(7) Å^3, Z = 4, D_c = 1.333 g cm^{-3}, μ = 0.820 mm^{-1}. F_{000} = 608, $2\theta_{max}$ = 152.7°, 29 337

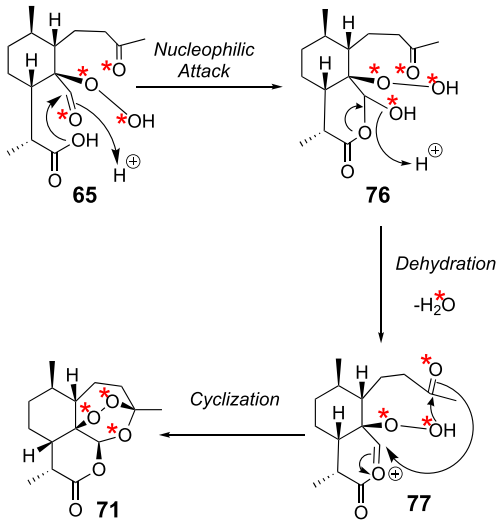

Figure 17. Alternative mechanistic pathway to artemisinin with three ^{18}O atoms (**71**) from intermediate **65**. *O = ^{18}O.

reflections collected, 2876 unique (R_{int} = 0.0392). Final GOOF = 1.099, R_1 = 0.0505, wR_2 = 0.1340, R indices based on 2770 reflections

https://doi.org/10.1021/acs.jnatprod.1c00246
J. Nat. Prod. 2021, 84, 1967−1984

Table 2. Summary of $^{18}O_2$ Incorporation into Artemisinin from d_3-DHAA (11)[a]

starting	time	$^{18}O_4$–artemisinin (Art) (58)[b]	$^{18}O_3$–Art (59)[b]	$^{18}O_2$–Art (60)[b]	$^{18}O_1$–Art (61)[b]	d_3-Art (14)
d_3-DHAA	71 h	1.44×10^8	7.31×10^7	1.02×10^7	5.68×10^5	4.64×10^6
	ratio =	255	129	18.0	1.00	8.17
d_3-DHAA	336 h	9.44×10^6	6.49×10^7	3.55×10^8	2.23×10^8	1.18×10^9
	ratio =	1.00	6.88	37.6	23.6	125

[a]Numbers reported are the areas under the peaks in the extracted ion chromatograms (retention time = 3.88 min corresponding to artemisinin, $^{18}O_4$–Art (58) = m/z 294, $^{18}O_3$–Art (59) = m/z 292, $^{18}O_2$–Art (60) = m/z 290, $^{18}O_1$–Art (61) = m/z 288, d_3-Art (14) = m/z 286). [b]All detected artemisinin isotopologues with ^{18}O atoms have three deuteriums.

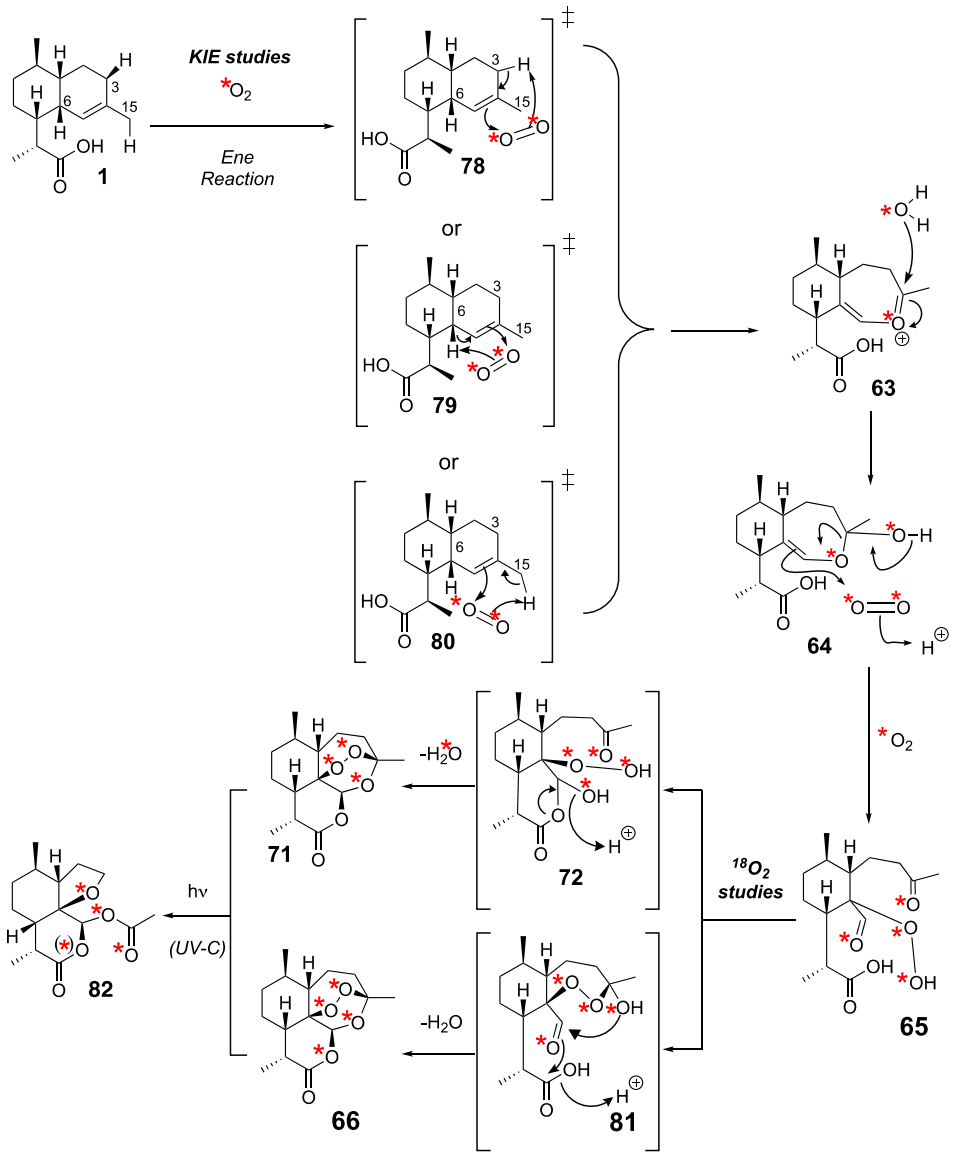

Figure 18. Summary of the mixed mechanism of artemisinin formation from DHAA (1) supported by KIE studies to show multiple ene reactions and $^{18}O_2$ labeling studies to show multiple polycyclization pathways to form the endoperoxide (66 and 71). *O = ^{18}O.

with $I > 2\sigma(I)$ (refinement on F^2), $|\Delta\rho|_{max}$= 0.283 e Å^{-3}, 184 parameters, 0 restraints.

X-ray Crystal Data for 22. From a solution of ethyl acetate:hexanes (1:1, v/v), 22 was obtained as colorless platelets. Crystallogrpahic data were collected at 98(2) K on a Rigaku AFC12/Saturn 724 CCD fitted using Mo K$_\alpha$, λ = 0.710 75 Å, followed by empirical absorption correction using spherical harmonics, implemented in SCALE3 ABSPACK[23] scaling algorithm. The structure was solved by direct methods (OLEX2[24] and ShelXT)[25] and refined against F^2 with full-matric least-squares using the program ShelXL.[26] All non-hydrogen atoms were refined with anisotropic displacement parameters. All H atoms, bound to carbon atoms, were placed on calculated positions and refined using the riding model with isotopic displacement parameters based on those of the parent atom. The oxygen bound hydrogen atom, H3, position was determined by electron density plot.

The crystallographic data can be obtained free of charge via https://www.ccdc.cam.ac.uk/structures/ or from the Cambridge Crystallographic Data Center, 12 Union Road, Cambridge CB2 1EZ, UK; fax: (+44)1223−336−033; or e-mail: deposit@ccdc.cam.ac.uk. CCDC number 2061810.

https://doi.org/10.1021/acs.jnatprod.1c00246
J. Nat. Prod. 2021, 84, 1967−1984

$C_{15}H_{24}O_3$, M = 252.34, 0.50 × 0.33 × 0.10 mm^3, orthorhombic, space group $P2_12_12_1$ (no. 19), a = 5.7974(5) Å, b = 14.3683(13) Å, c = 16.0292(13) Å, V = 1335.2(2) $Å^3$, Z = 4, D_c = 1.255 g cm^{-3}, μ = 0.085 mm^{-1}. F_{000} = 552, $2\theta_{max}$ = 50.1°, 2507 reflections collected, 2507 unique (R_{int} = 0.1619). Final GOOF = 1.063, R_1 = 0.0533, wR_2 = 0.1229, R indices based on 2180 reflections with $I > 2\sigma(I)$ (refinement on F^2), $|\Delta\rho|_{max}$= 0.281 e $Å^{-3}$, 157 parameters, 0 restraints.

X-ray Crystal Data for ***23***. From a solution of $CDCl_3$ (10 mg in 0.7 mL), **23** was obtained as colorless platelets. Crystallogrpahic data were collected at 100.0(1) K on a XtaLAB Synergy/Dualflex, HyPix fitted using Cu K_α, λ = 1.541 84 Å, followed by empirical absorption correction using spherical harmonics, implemented in SCALE3 ABSPACK[23] scaling algorithm. The structure was solved by direct methods (OLEX2[24] and ShelXT)[25] and refined against F^2 with full-matric least-squares using the program ShelXL.[26] All non-hydrogen atoms were refined with anisotropic displacement parameters. All hydrogen atoms were placed on calculated positions and refined using the riding model with isotopic displacement parameters based on those of the parent atom.

The crystallographic data can be obtained free of charge via https://www.ccdc.cam.ac.uk/structures/ or from the Cambridge Crystallographic Data Center, 12 Union Road, Cambridge CB2 1EZ, UK; fax: (+44)1223−336−033; or e-mail: deposit@ccdc.cam.ac.uk. CCDC number 2061811.

$C_{15}H_{28}O_3$, M = 256.37, 0.25 × 0.20 × 0.02 mm^3, triclinic, space group $P1$ (no. 1), a = 7.4494(4) Å, b = 9.7601(4) Å, c = 11.3665(6) Å, α = 76.475(4)°, β = 86.519(4)°, γ = 67.953(4)°, V = 744.41(7) $Å^3$, Z = 2, D_c = 1.144 g cm^{-3}, μ = 0.612 mm^{-1}. F_{000} = 284, $2\theta_{max}$ = 125.0°, 11 239 reflections collected, 3514 unique (R_{int} = 0.0706). Final GOOF = 1.111, R_1 = 0.0677, wR_2 = 0.1532, R indices based on 3254 reflections with $I > 2\sigma(I)$ (refinement on F^2), $|\Delta\rho|_{max}$= 0.345 e $Å^{-3}$, 337 parameters, 7 restraints.

■ ASSOCIATED CONTENT

Supporting Information

The Supporting Information is available free of charge at https://pubs.acs.org/doi/10.1021/acs.jnatprod.1c00246.

LC-HRMS and NMR analysis of DHAA isotopologues; 1D and 2D NMR data of compound **47**; description of time course experiments of DHAA to artemisinin; description of KIE experiments; description of experiments involving $^{18}O_2$ with DHAA; NMR spectra, high-resolution mass spectra, and IR spectra of synthesized compounds; HRMS data of time course experiments; HRMS data of KIE experiments; HRMS data of $^{18}O_2$ experiments; preliminary studies on the synthesis of 15,15,15-d_3-DHAA; X-ray crystallography data of compounds **1**, **2**, **22**, and **23**; and extra experiments to determine that benzoic acid can promote the conversion of DHAA to artemisinin (PDF)

Structure of **1** (CIF)

Structure of **2** (CIF)

Structure of **22** (CIF)

Structure of **23** (CIF)

■ AUTHOR INFORMATION

Corresponding Author

Francis K. Yoshimoto − *Department of Chemistry, The University of Texas at San Antonio (UTSA), San Antonio, Texas 78249-0698, United States;* orcid.org/0000-0002-2308-2999; Email: francis.yoshimoto@utsa.edu

Authors

Kaitlyn Varela − *Department of Chemistry, The University of Texas at San Antonio (UTSA), San Antonio, Texas 78249-0698, United States*

Hadi D. Arman − *Department of Chemistry, The University of Texas at San Antonio (UTSA), San Antonio, Texas 78249-0698, United States*

Complete contact information is available at: https://pubs.acs.org/10.1021/acs.jnatprod.1c00246

Notes

The authors declare no competing financial interest.

■ ACKNOWLEDGMENTS

This research was supported through the Bill & Melinda Gates Foundation [OPP1188432] and the Max and Minnie Tomerlin Voelcker Fund. Francis K. Yoshimoto PhD holds a Voelcker Fund Young Investigator Award from the MAX AND MINNIE TOMERLIN VOELCKER FUND. The UTSA RISE program is also acknowledged for supporting a research stipend for Ms. Kaitlyn Varela. NSF MRI grant for X-ray diffraction (Award No. 1920057) and NSF MRI grant for NMR spectrometer (Award No. 1625963) are also acknowledged. This manuscript is dedicated to Dr. Trevor Laird, on the occasion of his 75th birthday and for his guidance and support throughout this funded research project. We are truly grateful for the reviewers of this manuscript, who have significantly improved the quality of this paper by suggesting additional insightful experiments and providing their valuable, expert opinion.

■ REFERENCES

(1) Wallart, T. E.; van Uden, W.; Lubberink, H. G. M.; Woerdenbag, H. J.; Pras, N.; Quax, W. J. *J. Nat. Prod.* **1999**, *62*, 430−433.

(2) Pandey, A. V.; Tekwani, B. L.; Singh, R. L.; Chauhan, V. S. *J. Biol. Chem.* **1999**, *274*, 19383−19388.

(3) Krishna, S.; Bustamante, L.; Haynes, R. K.; Staines, H. M. *Trends Pharmacol. Sci.* **2008**, *29*, 520−527.

(4) Amara, Z.; Bellamy, J. F. B.; Horvath, R.; Miller, S. J.; Beeby, A.; Burgard, A.; Rossen, K.; Poliakoff, M.; George, M. W. *Nat. Chem.* **2015**, *7*, 489−495.

(5) Levesque, F.; Seeberger, P. H. *Angew. Chem., Int. Ed.* **2012**, *51*, 1706−1709.

(6) Lee, D. S.; Amara, Z.; Clark, C. A.; Xu, Z.; Kakimpa, B.; Morvan, H. P.; Pickering, S. J.; Poliakoff, M.; George, M. W. *Org. Process Res. Dev.* **2017**, *21*, 1042−1050.

(7) Demiray, M.; Tang, X.; Wirth, T.; Faraldos, J. A.; Allemann, R. K. *Angew. Chem., Int. Ed.* **2017**, *56*, 4347−4350.

(8) Elsherbini, M.; Allemann, R. K.; Wirth, T. *Chem. - Eur. J.* **2019**, *25*, 12486−12490.

(9) Krishna, S.; Woodrow, C. J.; Staines, H. M.; Haynes, R. K.; Mercereau-Puijalon, O. *Trends Mol. Med.* **2006**, *12*, 200−205.

(10) Eckstein-Ludwig, U.; Webb, R. J.; van Goethem, I. D. A.; East, J. M.; Lee, A. G.; Kimura, M.; O'Neill, P. M.; Bray, P. G.; Ward, S. A.; Krishna, S. *Nature* **2003**, *424*, 957−961.

(11) Bryant, L.; Flatley, B.; Patole, C.; Brown, G. D.; Cramer, R. *BMC Plant Biol.* **2015**, *15*, 175.

(12) Brown, G. D.; Sy, L.-K. *Tetrahedron* **2004**, *60*, 1139−1159.

(13) Sy, L.-K.; Brown, G. D. *Tetrahedron* **2002**, *58*, 897−908.

(14) Sy, L.-K.; Brown, G. D. *Tetrahedron* **2002**, *58*, 909−923.

(15) Acton, N.; Roth, R. J. *J. Org. Chem.* **1992**, *57*, 3610−3614.

(16) Varela, K.; Arman, H. D.; Yoshimoto, F. K. *J. Nat. Prod.* **2020**, *83*, 66−78.

(17) Rej, R. K.; Acharyya, R. K.; Nanda, S. *Tetrahedron* **2016**, *72*, 4931−4937.

(18) Lin, A. J.; Klayman, D. L.; Hoch, J. M.; Silverton, J. V.; George, C. F. *J. Org. Chem.* **1985**, *50*, 4504−4508.

(19) Adam, W.; Krebs, O.; Orfanopoulos, M.; Stratakis, M.; Vougiokalaki, G. C. *J. Org. Chem.* **2003**, *68*, 2420−2425.

(20) Singleton, D. A.; Hang, C.; Szymanski, M. J.; Meyer, M. P.; Leach, A. G.; Kuwata, K. T.; Chen, J. S.; Greer, A.; Foote, C. S.; et al. *J. Am. Chem. Soc.* **2003**, *125*, 1319−1328.
(21) Alberti, M. N.; Orfanopoulos, M. *Chem. - Eur. J.* **2010**, *16*, 9414−9421.
(22) Harding, L. B.; Goddard, W. A. *J. Am. Chem. Soc.* **1980**, *102*, 439−449.
(23) *SCALE3 ABSPACK—An Oxford Diffraction program* (1.0.4, g.); Oxford Diffraction Ltd., 2005.
(24) Dolomanov, O. V.; Bourhis, L. J.; Gildea, R. J.; Howard, J. A. K.; Puschmann, H. *J. Appl. Crystallogr.* **2009**, *42*, 339−341.
(25) Sheldrick, G. M. *Acta Crystallogr., Sect. A: Found. Adv.* **2015**, *A71*, 3−8.
(26) Sheldrick, G. M. *Acta Crystallogr., Sect. A: Found. Crystallogr.* **2008**, *A64*, 112−122.

https://doi.org/10.1021/acs.jnatprod.1c00246
J. Nat. Prod. 2021, 84, 1967−1984